Applied Ocean Research 78 (2018) 201–211

Contents lists available at ScienceDirect

Applied Ocean Research

journal homepage: www.elsevier.com/locate/apor

QUUV: A quadrotor-like unmanned underwater vehicle with thrusts configured as X shape☆

Jingwei Bian, Ji Xiang*

National Laboratory of Industrial Control Technology, and College of Electrical Engineering, Zhejiang University, Hangzhou, China

ARTICLE INFO

Keywords:
Quadrotor-like unmanned underwater vehicle (QUUV)
X shape
Motion analysis
Sliding mode controller

ABSTRACT

A quadrotor-like unmanned underwater vehicle (QUUV) is presented in this paper. The four fixed thrusters are configured as *X* shape through which the QUUV has vertical and horizontal movements decoupled. Its mathematical model and motion analysis are introduced accordingly. The differences with conventional underwater vehicles are also discussed to show its merits. Sliding mode control is adopted to design its controller. Various motions with the sliding mode controller are simulated, followed by an experiment test in a small pool.

1. Introduction

Nowadays, unmanned underwater vehicles have been an valuable tool for underwater exploration and operation with the growing importance of the ocean. It is an effective instrument to replace human beings in the unknown and hazardous underwater environment. In past decades many kinds of unmanned underwater vehicles (UUVs) have been designed and implemented for various applications, such as coastal oceanography [1], underwater cable examination [2], underwater archaeology [3].

There are mainly two kinds of shape configuration for UUV. One is open structure shape. Almost all remotely operated vehicles (ROV) adopt this shape configuration. The underwater vehicles with open structure are often cuboid shape. It has the advantage of large load capacity and can stay in the water for a long period with an umbilical cable to carry power from the mother-ship. The JASON ROV developed at the Woods Hole Oceanographic Institution can perform scientific tasks on the seafloor to depths of 6000 m [4]. The deep ROV Dolphin-3K is used to study colonies of giant clams, tube worms and geology of steep cliffs studies, which was manufactured by Japan Marine Science and Technology Center [5]. One disadvantage of these ROV is that its maneuverability and hydrodynamic property are not good because of its umbilical cable and cuboid shape.

The other is torpedo-like shape, which is common for autonomous underwater vehicles (AUV). It often has only a thruster at the tail and turns with the help of rudders or fins. In [6] a generation of autonomous underwater vehicle, named REMUS, is presented by the Woods Hole Oceanographic Institution; it has developed multiple series for different depth. In [7], a small AUV named ISiMI is designed to cruise the ocean engineering basin by The Korea Ocean Research and Development Institute. REMUS and ISiMI both have torpedo-like shape and have only a thruster with rudders or fins. They have to move in the horizontal direction when moving in the vertical direction, which make their motion performance not good.

There have been some multi-thruster unmanned underwater vehicles considering merits and weakness mentioned above. An advanced underwater vehicle is presented in [8,9] and adopts nearly spherical shape with eight thrusters, named omni-Directional Intelligent Navigator (ODIN). Its maneuverability and hydrodynamic property is better. In [10] thruster configurations are discussed and a better thruster configuration with six thrusters is proposed in theory. These multi-thruster underwater vehicles often have six to eight thrusters, which are relatively redundant for common motion, such as heave motion, surge motion and cruise motion. So far there are about more than 100 prototypes in the laboratories all over the world as mentioned in [11]. More kinds of underwater vehicles can refer to [12,13] and other literature.

Recently some reports about submersible unmanned aerial vehicles (UAV) have been made, which are apparently different from UUVs mentioned above. Their motivation is to offer a new kind of underwater vehicle with better performance based on UAV technology. There are two kinds of submersible UAV: submersible fixed-wing UAV and quadrotor UAV [14,15]. In [16] a submersible unmanned aerial vehicle (UAV) with fixed-wings is proposed, and its impact force with water is

☆ This research is supported by the National Natural Science Foundation of China (61773339), the Fundamental Research Funds for the Central Universities (2018XZZX001-06), and the Research Project of the state key Laboratory of Industrial Control Technology (ICT1811).

* Corresponding author.
E-mail address: jxiang@zju.edu.cn (J. Xiang).

https://doi.org/10.1016/j.apor.2018.06.017
Received 8 July 2017; Received in revised form 29 May 2018; Accepted 20 June 2018
Available online 30 June 2018
0141-1187/

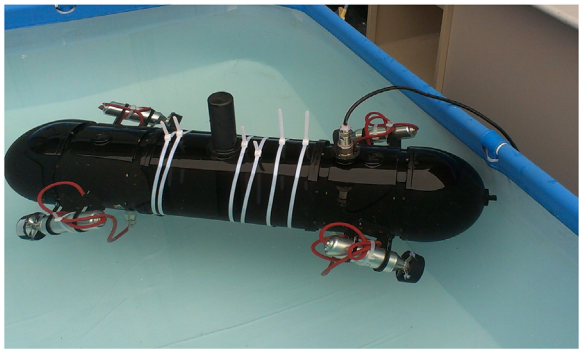

Fig. 1. The QUUV prototype.

calculated by the method of the computational fluid dynamics (CFD). In [17] a particular submersible fixed-wing UAV has been investigated and studied in detail. In addition, quadrotor UAV has become a commercial UAV because of its simple structure and flexible movement. Some researchers have studied quadrotor UAV applied in the water. In [18] a submersible quadrotor-like unmanned aerial underwater vehicle is proposed, and its kinematic and dynamic models are presented. In [19] an underwater vehicle with a quadrotor configuration is designed, and its controllers are simulated. They adopt directly thrusters configuration of the quadrotor UAV, which are upright. Their works neglect the difference between air motion and underwater motion. Thrusters configuration should be redesigned to fit with underwater situation.

This paper, as an extension of conference version [20], formally proposes a quadrotor-like unmanned underwater vehicle (QUUV). As shown in Fig. 1 the significant improvement is that four thrusters of the QUUV are inclined in this paper, which are distributed at two sides of the hull with a constant angle to form a so-called *X* shape. Moreover, controllers are designed directly to the thrust force. In comparison with underwater vehicles mentioned above, the QUUV has its special characteristics as below:

- Its motion performance is better than torpedo-like AUV. It can hover in a position and move in the vertical direction and horizontal direction independently, which cannot be achieved by torpedo-like AUV. In addition, it can yaw in a position. These good benefits attribute to the four inclined thrusters, which will be described in details in next section. Its maneuverability is better than torpedo-like AUVs because of four thrusters offering more degree of freedom for control.
- Its maneuverability and hydrodynamic property are better than conventional ROVs. In comparison with ROVs with open structure, the QUUV have a streamline shape and need not tether to the mother-ship, which make the QUUV have better maneuverability and hydrodynamic property. In addition, the QUUV with four thrusters can achieve the same flexible motion as conventional ROVs.
- Its design fits with in underwater application well. In the air, the thrusters are mainly used to overcome the gravity for the quadrotor UAV. However, the gravity of the vehicles is equal to or slightly less than the buoyancy in the water. The thrusters need to be mainly used to overcome surge resistance in the water because of large water density. The X shape of the QUUV makes the power of thrusts mainly against surge resistance.

To sum up, the QUUV avoids some aforementioned shortcomings of conventional underwater vehicles and has some advantages on maneuverability and adaptability to underwater motion. Compared to multi-thruster underwater vehicles designs, such as those in [8–10], the QUUV can achieve flexible motion with fewer thrusters, which is shown by space motion in Section 6. The QUUV is a better design considering maneuverability, hydrodynamic property and other qualities in comparison with conventional underwater vehicles.

The paper is organized as follows. Section 2 describes the design and *X* shape of the QUUV. In Section 3 the mathematical model of the QUUV is established, and some differences with conventional unmanned underwater vehicles are disclosed. The motion analysis is discussed in Section 4. The sliding mode controller design is introduced in Section 5, and various motion simulation results based on sliding mode are shown in Section 6. An experiment test is carried out based on a simple path planning in Section 7. Finally, a conclusion is drawn in Section 8.

2. System design of the QUUV

2.1. Overview of the QUUV

The QUUV addressed in this paper has a prototype shown in Fig. 1. It is composed of mechanical body, control system, communication system and power system. The mechanical body contains hull structure and four thrusters as *X* shape. The control system contains digital signal processor, sensors and other related electronic equipment. The communication system includes radio communication and acoustic communication. The power system adopts lithium battery. Table 1 shows the overall design parameters and its specification.

The control system is the most important part of the prototype. The digital signal processor is adopted in this prototype. The attitude and heading reference system (AHRS) provides information of the 3-axis angular velocities, 3-axis accelerations and 3-axis magnetic intensity to the digital signal processor. The AHRS is composed of a six-axis (gyro& accelerometer) MEMS device, a three-axis magnetometer and an ARM micro-controller. The depth information is gathered by the pressure sensor. The thrusters adopt brushless motors that are controlled by electronic speed controllers connecting with the digital signal processor. The thruster is powered by 12 V. Its maximum speed and thrust are 14,000 rpm and 4 kg, respectively.

The QUUV has two ways to communicate with the computer on land or on board. A wireless radio antenna is installed at the top of the hull, and an underwater acoustic transducer is installed at the front end of the hull. When the QUUV is on the water surface radio communication is applied. When the QUUV is underwater, acoustic communication is used because radio communication will encounter severe attenuation problems.

The lithium battery supplies all the system with power, which is arranged at the bottom of the prototype so that the center of gravity is below the center of buoyancy.

2.2. X shape

The hull size of the QUUV is constrained by the space for the instruments, and the hull shape is constrained by the hydrodynamic characteristics. The hull shape of the QUUV is designed based on the Myring hull profile equations which are known for minimizing the drag force [21]. What's more, as shown in Fig. 2, there are four thrusters symmetrically distributed at two sides of the hull. There is an angle β ($0^\circ < \beta < 90^\circ$) representing the angle between the hull and the thruster as depicted in Fig. 2, named as thruster angle. The thrusters at the right side cross the thrusters at the left side to form *X* shape, as depicted by blue line in Fig. 2. It is stated that the angle β is fixed when

Table 1
Design parameters and specifications.

Mass in air	45 kg
Total volume	45.2 dm^3
Total length	1.2 m
Diameter	25 cm
Design velocity	2 m/s

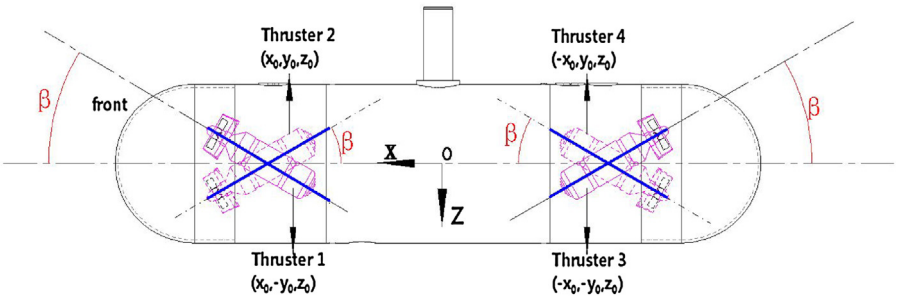

Fig. 2. The left side view schematic of the QUUV.

the QUUV moves in the water. Considering motion requirements and hydrodynamic resistance, the angle β can be found a optimized value, which will be further studied in the future. Such an X shape offer an interesting distribution of the four thrusters, which makes the coupled six-degree motion decompose into four kind of motion, namely heave motion, surge motion, roll motion, pitch and yaw motion. The detailed motion analysis of the four thrusters as X shape will be detailed in Section 4.

3. Mathematical modelling

3.1. Mathematical modelling

As indicted in [22,23], an underwater vehicle can be completely described by its position and orientation with respect to the earth-fixed coordinate system. It is convenient to define two coordinate frames as shown in Fig. 3 to analyze the QUUV. The coordinate frame $\{\mathbf{E}\} := \{X, Y, Z\}$ is the earth-fixed coordinate (inertial coordinate) and $\{\mathbf{B}\} := \{x, y, z\}$ is the vehicle-fixed coordinate. The following notation will be used in the rest of this paper. The pose vector of the vehicle is represented by $\boldsymbol{\eta} = [\boldsymbol{\eta_1}^T, \boldsymbol{\eta_2}^T]^T$, where $\boldsymbol{\eta_1} = [X, Y, Z]^T$ is the position vector and $\boldsymbol{\eta_2} = [\phi, \theta\, \psi]^T$ is the orientation vector with respect to the earth-fixed coordinate in the earth-fixed coordinate system. $\mathbf{v}$ expresses the velocity vector with respect to the origin of the earth-fixed coordinate in the vehicle-fixed coordinate system represented by $\mathbf{v} = [\mathbf{v_1}^T, \mathbf{v_2}^T]^T$. Let $\mathbf{v_1} = [u, v, w]^T$ be the linear velocity vector and let $\mathbf{v_2} = [p, q, r]^T$ be the angular velocity vector. The six variables represent six velocity components of motion, namely surge, sway, heave, roll, pitch, and yaw.

The kinematic equation can be given by

$$\dot{\boldsymbol{\eta}} = \mathbf{J}(\boldsymbol{\eta_2})\mathbf{v}. \tag{1}$$

Here $\mathbf{J}(\boldsymbol{\eta_2})$ is a velocity transformation matrix that transforms velocities of the vehicle-fixed to the earth-fixed coordinate frame as given by,

$$\mathbf{J}(\boldsymbol{\eta_2}) = \begin{bmatrix} \mathbf{J_1}(\boldsymbol{\eta_2}) & \mathbf{0}_{3\times3} \\ \mathbf{0}_{3\times3} & \mathbf{J_2}(\boldsymbol{\eta_2}) \end{bmatrix}_{6\times6}, \tag{2}$$

$$\mathbf{J_1}(\boldsymbol{\eta_2}) = \begin{bmatrix} c_\psi c_\theta & c_\psi s_\theta s_\phi - s_\psi c_\phi & c_\psi s_\theta c_\phi + s_\psi s_\phi \\ s_\psi c_\theta & s_\psi s_\theta s_\phi + c_\psi c_\phi & s_\psi s_\theta c_\phi - c_\psi s_\phi \\ -s_\theta & c_\theta s_\phi & c_\theta c_\phi \end{bmatrix}, \tag{3}$$

$$\mathbf{J_2}(\boldsymbol{\eta_2}) = \begin{bmatrix} 1 & s_\phi t_\theta & c_\phi t_\theta \\ 0 & c_\phi & -s_\phi \\ 0 & s_\phi/c_\theta & c_\phi/c_\theta \end{bmatrix}, \tag{4}$$

where $c_{(\cdot)}$, $s_{(\cdot)}$ and $t_{(\cdot)}$ are short notations for cos(·), sin(·) and tan(·) throughout of this paper, respectively. The dynamics equation can be written as [23]:

$$\begin{aligned} &\mathbf{M}\dot{\mathbf{v}} + \mathbf{C}(\mathbf{v})\mathbf{v} + \mathbf{D}(\mathbf{v})\mathbf{v} + \mathbf{g}(\boldsymbol{\eta}) = \boldsymbol{\tau} + \mathbf{w}, \\ &\boldsymbol{\tau} = \mathbf{B}\mathbf{u}, \end{aligned} \tag{5}$$

where $\mathbf{M}$ is a 6 × 6 inertia matrix as a sum of the rigid body inertia matrix $\mathbf{M_R}$ and the hydrodynamic virtual inertia (added mass) $\mathbf{M_A}$; $\mathbf{C}(\mathbf{v})$ is a 6 × 6 Coriolis and centripetal matrix including rigid body terms $\mathbf{C_R}(\mathbf{v})$ and terms $\mathbf{C_A}(\mathbf{v})$ due to the added mass; $\mathbf{D}(\mathbf{v})$ is a 6 × 6 damping matrix including terms due to drag forces; $\mathbf{g}(\boldsymbol{\eta})$ is a 6 × 1 vector containing the restoring terms formed by the vehicles buoyancy and gravitational terms; $\boldsymbol{\tau}$ is a 6 × 1 vector including the control forces and moments, namely $[\tau_X, \tau_Y, \tau_Z, \tau_K, \tau_M, \tau_N]^T$, which is produced by four

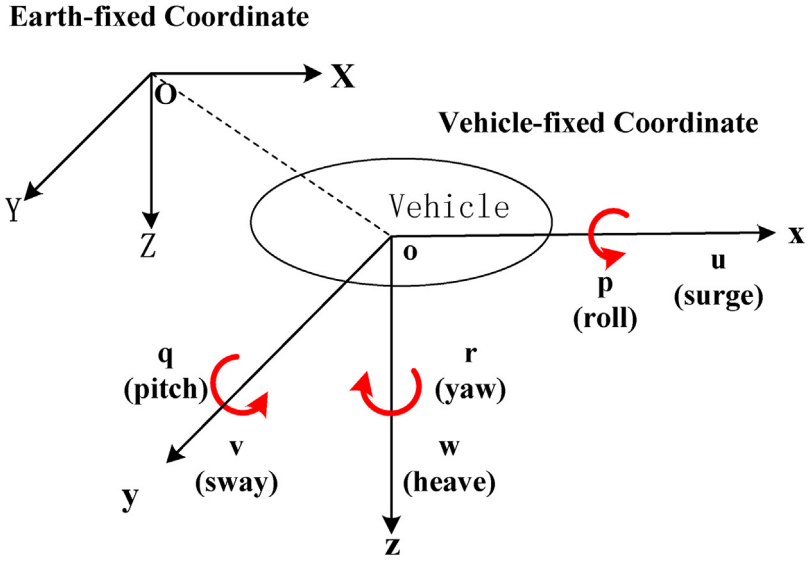

Fig. 3. The coordinate frames [24].

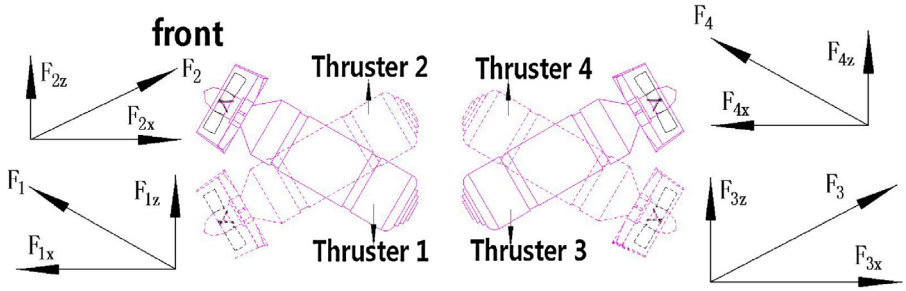

Fig. 4. The heave motion.

thrusters; **w** is a 6×1 disturbance vector representing the environmental forces and moments acting on the vehicle; **B** is a control matrix of appropriate dimensions and **u** is a vector whose components are thruster forces.

As for **B** and **u** for the QUUV, in order to describe the problem better, we make the following assumptions.

- The position of the four thrusters is symmetric about x-axis and y-axis in the vehicle-fixed coordinate as well as at the same height, namely $(x_0, -y_0, z_0)$, (x_0, y_0, z_0), $(-x_0, -y_0, z_0)$, $(-x_0, y_0, z_0)$ as shown in Fig. 2. In addition let $z_0 = 0$.
- As shown in Fig. 4 the forces F_i produced by four thrusters has only components along x-axis and z-axis. The corresponding magnitude of the force and moment for six degree of freedom motion is denoted as:

  $F_{ix}, F_{iz}, K_i, M_i, N_i$

  where $i = 1, 2, 3, 4$, represent four thrusters, respectively. It is defined that if $F_i > 0$ the thruster i actuates in the clockwise direction. If $F_i < 0$ the thruster i actuates in the counter-clockwise direction. Fig. 6 shows the orientation of F_i when $F_i < 0$.
- The origin of the vehicle-fixed coordinate coincides with the center of gravity.
- The center of buoyancy is higher than the center of gravity.

With the above assumptions, the following can be obtained,

$$\mathbf{u} = [F_1, F_2, F_3, F_4]^T, \tag{6}$$

$$\mathbf{B} = \begin{bmatrix} -c_\beta & -c_\beta & c_\beta & c_\beta \\ 0 & 0 & 0 & 0 \\ s_\beta & -s_\beta & s_\beta & -s_\beta \\ -y_0 s_\beta & -y_0 s_\beta & -y_0 s_\beta & -y_0 s_\beta \\ -z_0 c_\beta - x_0 s_\beta & -z_0 c_\beta + x_0 s_\beta & z_0 c_\beta + x_0 s_\beta & z_0 c_\beta - x_0 s_\beta \\ -y_0 c_\beta & y_0 c_\beta & y_0 c_\beta & -y_0 c_\beta \end{bmatrix}. \tag{7}$$

3.2. Hydrodynamic modelling description

The hydrodynamic virtual inertia (added mass) matrix $\mathbf{M_A}$ can be written as [24]:

$$\mathbf{M_A} \triangleq -\begin{bmatrix} X_{\dot u} & X_{\dot v} & X_{\dot w} & X_{\dot p} & X_{\dot q} & X_{\dot r} \\ Y_{\dot u} & Y_{\dot v} & Y_{\dot w} & Y_{\dot p} & Y_{\dot q} & Y_{\dot r} \\ Z_{\dot u} & Z_{\dot v} & Z_{\dot w} & Z_{\dot p} & Z_{\dot q} & Z_{\dot r} \\ K_{\dot u} & K_{\dot v} & K_{\dot w} & K_{\dot p} & K_{\dot q} & K_{\dot r} \\ M_{\dot u} & M_{\dot v} & M_{\dot w} & M_{\dot p} & M_{\dot q} & M_{\dot r} \\ N_{\dot u} & N_{\dot v} & N_{\dot w} & N_{\dot p} & N_{\dot q} & N_{\dot r} \end{bmatrix} \tag{8}$$

with the notation of SNAME (The Society of Naval Architects and Marine Engineers). For example the hydrodynamic force X_A along the x-axis due to an acceleration in the x-direction is written as [24]:

$$X_A = X_{\dot u}\dot u \quad \text{with} \quad X_{\dot u} \triangleq \frac{\partial X}{\partial \dot u} \tag{9}$$

where X is the hydrodynamic virtual inertia force along the x-axis. In general, $\mathbf{M_A}$ is strictly positive and symmetrical. Coriolis and centripetal matrix $\mathbf{C_A}$ due to added mass can be obtained according to $\mathbf{M_A}$. For some geometrical structure, $\mathbf{M_A}$ can be simplified. For instance, the torpedo-like underwater vehicles often have a structure symmetric with respect to x–z plane (port/starboard) for which $\mathbf{M_A}$ can be simplified as [23]:

$$\mathbf{M_A} = -\begin{bmatrix} X_{\dot u} & 0 & X_{\dot w} & 0 & X_{\dot q} & 0 \\ 0 & Y_{\dot v} & 0 & Y_{\dot p} & 0 & Y_{\dot r} \\ Z_{\dot u} & 0 & Z_{\dot w} & 0 & Z_{\dot q} & 0 \\ 0 & K_{\dot v} & 0 & K_{\dot p} & 0 & K_{\dot r} \\ M_{\dot u} & 0 & M_{\dot w} & 0 & M_{\dot q} & 0 \\ 0 & N_{\dot v} & 0 & N_{\dot p} & 0 & N_{\dot r} \end{bmatrix}. \tag{10}$$

In this case, the dynamic model (5) can be separated into two lightly interacting subsystems: (u, w, q) and(v, p, r), which have been widely adopted to design controllers for torpedo-like underwater vehicles.

However, the QUUV here is symmetric with respect to the $y - z$ plane (fore/aft), and its $\mathbf{M_A}$ is simplified as:

$$\mathbf{M_A} = -\begin{bmatrix} X_{\dot u} & 0 & 0 & 0 & X_{\dot q} & X_{\dot r} \\ 0 & Y_{\dot v} & Y_{\dot w} & Y_{\dot p} & 0 & 0 \\ 0 & Z_{\dot v} & Z_{\dot w} & Z_{\dot p} & 0 & 0 \\ 0 & K_{\dot v} & K_{\dot w} & K_{\dot p} & 0 & 0 \\ M_{\dot u} & 0 & 0 & 0 & M_{\dot q} & M_{\dot r} \\ N_{\dot u} & 0 & 0 & 0 & N_{\dot q} & N_{\dot r} \end{bmatrix}. \tag{11}$$

Correspondingly, the dynamic model of the QUUV can be separated into two lightly interacting subsystems: (u, q, r) and (v, w, p). Then it can be seen that heave motion (w) and surge motion (u) are independent for the QUUV. While, heave motion (w) and surge motion (u) have the close relationship with each other for torpedo-like AUVs. In fact, the heave motion (w) relies on the surge motion (u) for torpedo-like AUVs. The independent heave motion and surge motion offer better maneuverability for the QUUV in contrast with torpedo-like AUVs. More detailed descriptions can be found in Section 6.

4. Motion analysis

This section will detail the mechanism of the six-DOF (degree of freedom) space motion in order to demonstrate the merit of distribution of the four thrusters as an X shape. It is noticed that the buoyancy is equal to or slightly larger than the gravity. Because of the forces produced by four thrusters having value along x-axis and z-axis, it should be noted that the sway motion cannot be achieved, which will not be discussed.

4.1. Heave motion

Let $F_1 = F_3 = -F_2 = -F_4$ and $F_1 < 0$ for the heave motion as shown in Fig. 4. It leads to $\tau_X = 0$, $\tau_Y = 0$ and $\tau_Z \neq 0$. The resultant force acts vertically upward. In addition, it can be obtained:

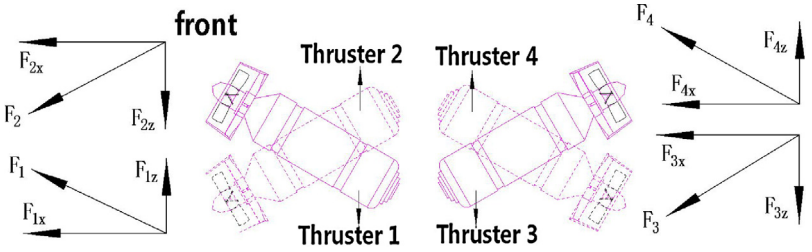

Fig. 5. The surge motion.

$$\begin{aligned}
\tau_K=&\ |F_{1z}|y_0 - |F_{2z}|y_0 + |F_{3z}|y_0 - |F_{4z}|y_0 = 0,\\
\tau_M=&\ (|F_{1x}|z_0 + |F_{1z}|x_0) + (-|F_{2x}|z_0 + |F_{2z}|x_0)\\
&+ (-|F_{3x}|z_0 - |F_{3z}|x_0) + (|F_{4x}|z_0 - |F_{4z}|x_0)\\
=&\ 0,\\
\tau_N=&\ |F_{1x}|y_0 + |F_{2x}|y_0 - |F_{3x}|y_0 - |F_{4x}|y_0 = 0.
\end{aligned} \tag{12}$$

According to Newton's laws, the underwater vehicle moves vertically upward.

Let $F_1 = F_3 = -F_2 = -F_4$ and $F_1 > 0$ for the heave motion. Motion analysis is alike. If $\tau_Z > B - W$ the underwater vehicle moves vertically downward. If $\tau_Z = B - W$ the underwater vehicle keeps hovering. If $\tau_Z < B - W$ the underwater vehicle moves vertically upward.

4.2. Surge motion

For the surge motion there are two situations considering buoyancy (B) and weight (W). When $B = W$, let $F_1 = F_2 = -F_3 = -F_4$ and $F_1 < 0$ as shown in Fig. 5. It leads to $\tau_Z = 0$, $\tau_Y = 0$ and $\tau_X \neq 0$. In addition, it can be obtained:

$$\begin{aligned}
\tau_K=&\ |F_{1z}|y_0 + |F_{2z}|y_0 - |F_{3z}|y_0 - |F_{4z}|y_0 = 0,\\
\tau_M=&\ (|F_{1x}|z_0 + |F_{1z}|x_0) + (|F_{2x}|z_0 - |F_{2z}|x_0)\\
&+ (|F_{3x}|z_0 + |F_{3z}|x_0) + (|F_{4x}|z_0 - |F_{4z}|x_0)\\
=&\ (|F_{1x}| + |F_{2x}| + |F_{3x}| + |F_{4x}|)z_0 = 0,\\
\tau_N=&\ |F_{1x}|y_0 - |F_{2x}|y_0 + |F_{3x}|y_0 - |F_{4x}|y_0 = 0.
\end{aligned} \tag{13}$$

Since only τ_x exists, the underwater vehicle can move forward without heave motion. When $B > W$, let $F_1 = -F_4$, $F_2 = -F_3$, $F_1 < 0$, $F_2 < 0$ and $(|F_2| - |F_1|)\sin(\beta) = B - W$ in order to counteract the buoyancy. Other analysis is alike.

If the four thrusters force F_i are only positive and negative opposite in contrast with them stated before, the underwater vehicle will move backward without heave motion.

4.3. Roll motion

For roll motion there are also two situations considering buoyancy (B) and weight (W). When $B = W$, let $F_1 = F_2 = F_3 = F_4$ and $F_1 < 0$ as shown in Fig. 6. It leads to $\tau_X = 0$, $\tau_Y = 0$ and $\tau_Z = 0$. In addition, it can be obtained:

$$\begin{aligned}
\tau_K=&\ |F_{1z}|y_0 + |F_{2z}|y_0 + |F_{3z}|y_0 + |F_{4z}|y_0\\
=&\ (|F_{1z}| + |F_{2z}| + |F_{3z}| + |F_{4z}|)y_0,\\
\tau_M=&\ (|F_{1x}|z_0 + |F_{1z}|x_0) + (|F_{2x}|z_0 - |F_{2z}|x_0)\\
&+ (-|F_{3x}|z_0 - |F_{3z}|x_0) + (-|F_{4x}|z_0 + |F_{4z}|x_0)\\
=&\ 0,\\
\tau_N=&\ |F_{1x}|y_0 - |F_{2x}|y_0 - |F_{3x}|y_0 + |F_{4x}|y_0 = 0.
\end{aligned} \tag{14}$$

Again the roll movement can be achieved independently. When $B > W$, let $F_1 = F_3$, $F_2 = F_4$, $F_1 < 0$, $F_2 < 0$ and $(|F_2| - |F_1|)\sin(\beta) = B - G$ in order to counteract the buoyancy. The same motion results can be obtained by similar analysis.

4.4. Pitch and yaw motion

For pitch and yaw motion there are still two situations considering buoyancy (B) and weight (W). When $B = W$, $F_1 = F_4 = -F_2 = -F_3$ and $F_1 > 0$ as shown in Fig. 8. It can be seen that $\tau_X = 0$, $\tau_Y = 0$ and $\tau_Z = 0$. In addition, it can be obtained:

$$\begin{aligned}
\tau_K=&\ -|F_{1z}|y_0 + |F_{2z}|y_0 + |F_{3z}|y_0 - |F_{4z}|y_0 = 0,\\
\tau_M=&\ (-|F_{1x}|z_0 - |F_{1z}|x_0) + (|F_{2x}|z_0 - |F_{2z}|x_0)\\
&+ (-|F_{3x}|z_0 - |F_{3z}|x_0) + (|F_{4x}|z_0 - |F_{4z}|x_0)\\
=&\ -(|F_{1z}| + |F_{2z}| + |F_{3z}| + |F_{4z}|)x_0,\\
\tau_N=&\ -|F_{1x}|y_0 - |F_{2x}|y_0 - |F_{3x}|y_0 - |F_{4x}|y_0\\
=&\ -(|F_{1x}| + |F_{2x}| + |F_{3x}| + |F_{4x}|)y_0.
\end{aligned} \tag{15}$$

It can be seen from (15) that pitch and yaw motion are coupled. But it can be achieved in a relatively independent way to yaw in a position with the help of buoyancy moment. As shown in Fig. 7 the underwater vehicle will produce buoyancy moment when having pitch angle. The buoyancy moment has the opposite direction with the pitch moment (τ_M). The buoyancy moment can make the pitch angle return to zero during and after yaw motion.

When $B > W$, let $F_1 = -F_2$, $F_3 = F_4$, $F_1 > 0$, $F_3 < 0$ and $(|F_1| - |F_3|)\sin(\beta) = B - W$ in order to counteract the buoyancy. The same motion results can be obtained because of similar analysis.

5. Controller design

The sliding mode control has been successfully applied to the control of underwater vehicles as shown in [25–27] because of its strong robustness to uncertain parameters and disturbances. Sliding mode controllers principle for the QUUV system will be presented in this

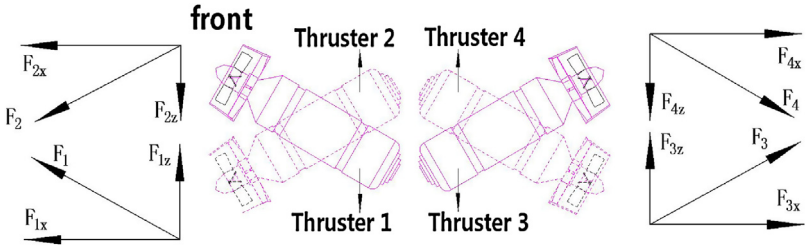

Fig. 6. The roll motion.

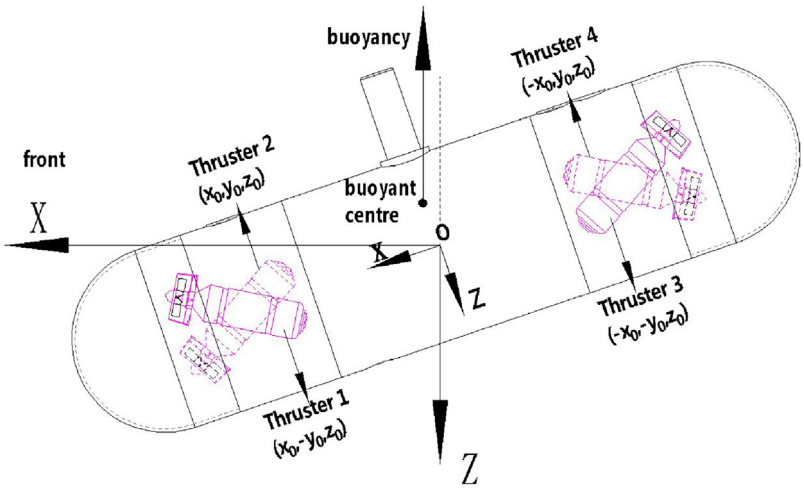

Fig. 7. Buoyancy moment when having pitch angle.

section.

It is analogous to that in [28] that the QUUV system can be written in the form:

$$\dot{\mathbf{x}} = \mathbf{Ax} + \mathbf{Bu} + f(\mathbf{x}, t) \tag{16}$$

where $\mathbf{x} \in R^{n\times 1}$, $\mathbf{A} \in R^{n\times n}$, $\mathbf{B} \in R^{n\times m}$, $\mathbf{u} \in R^{m\times 1}$, and $f(\mathbf{x}, t) \in R^{n\times 1}$ is a nonlinear function describing disturbances and unmodelled dynamics. Firstly consider a usual sliding surface:

$$\boldsymbol{\sigma}(\tilde{\mathbf{x}}) = \mathbf{H}^{\mathbf{T}}\tilde{\mathbf{x}} = [\sigma_1, \sigma_2, ..., \sigma_m]^T \tag{17}$$

where $\mathbf{H} \in R^{n\times m}$ is a design matrix, $\tilde{\mathbf{x}} = \mathbf{x} - \mathbf{x_d}$ and $\boldsymbol{\sigma} \in R^{m\times 1}$. Let

$$\mathbf{H^T Bu} = [\mathbf{H^T}\dot{\mathbf{x}}_\mathbf{d} - \mathbf{H^T Ax} - \mathbf{H^T}f(\mathbf{x}, t) - \mathbf{F}] \tag{18}$$

where $\mathbf{F} \in R^{m\times 1}$ is given by

$$\mathbf{F} = [\xi \tanh(\sigma_1/\rho), \xi \tanh(\sigma_2/\rho), ..., \xi \tanh(\sigma_m/\rho)]^T \tag{19}$$

for two positive scalars $\xi > 0$ and $\rho > 0$. Then

$$\dot{\sigma}(\tilde{\mathbf{x}}) = -\mathbf{F}. \tag{20}$$

Consider the Lyapunov function:

$$V(\boldsymbol{\sigma}) = \frac{1}{2}\sigma_1^2 + \frac{1}{2}\sigma_2^2 + ... + \frac{1}{2}\sigma_m^2. \tag{21}$$

It can be obtained that:

$$\begin{aligned} \dot{V}(\mathbf{x}, t) &= \sigma_1\dot{\sigma}_1 + \sigma_2\dot{\sigma}_2 + ... + \sigma_m\dot{\sigma}_m \\ &= -\xi\sigma_1 \tanh(\sigma_1/\rho) - \xi\sigma_2 \tanh(\sigma_2/\rho) - \cdots - \xi\sigma_m \tanh(\sigma_m/\rho) \\ &\le 0. \end{aligned} \tag{22}$$

Therefore, according to Barbalat lemma, $\boldsymbol{\sigma}$ will converge to zero in finite time. The scalar ξ is chosen to large enough to overcome the destabilizing effects of any disturbance and mismatch, but ξ has a poor effect on dynamic performance if it has a improper large value. The magnitude of ξ will be a trade-off between robustness and performance. The magnitude of ρ is selected to eliminate control chattering, as described in [25,29].

It is noted that $\mathbf{H^T B}$ may be not a square matrix and thereby $\mathbf{u}$ may have multiple solutions for Eq. (18). Let $\mathbf{H}_1 = \mathbf{h^T}\dot{\mathbf{x}}_\mathbf{d} - \mathbf{H^T Ax} - \mathbf{H^T}f(\mathbf{x}, t) - \mathbf{F}$ and $\mathbf{H}_2 = \mathbf{H^T B}$. Eq. (18) can be rewritten:

$$\mathbf{H}_2\mathbf{u} = \mathbf{H}_1. \tag{23}$$

In fact roll and pitch motion are always neglected considering buoyancy moment [30]. It is essential to find a specific solution to minimize τ_K and τ_M, that is minimizing the scalar index f:

$$f = \mathbf{u}^T\mathbf{B}_4^T\mathbf{B}_4\mathbf{u} + \mathbf{u}^T\mathbf{B}_5^T\mathbf{B}_5\mathbf{u}. \tag{24}$$

where $\mathbf{B}_i (i = 1, 2, 3, 4, 5, 6)$ represents the i-th row of $\mathbf{B}$. The method of Lagrange multiplier optimality is adopted for minimizing f with the equality constraint ($\mathbf{H}_2\mathbf{u} = \mathbf{H}_1$). The specific example can be seen in next section.

6. Simulation

As mentioned above horizontal and vertical motion are independent for the QUUV because of independent heave and surge motion. These facts will be demonstrated by the surge and heave motion simulation. In addition, three-dimensional space motion is the basic and most important motion for underwater vehicles. It will be discussed at last. Table 2 gives some hydrodynamics coefficients and parameters that controllers design needs. It is admitted that the number of hydrodynamics coefficients is more than 12. Considering some hydrodynamics coefficients with small value, 12 hydrodynamics coefficients with relatively large value are presented in Table 2. All the hydrodynamics Coefficients are obtained with numerical computation

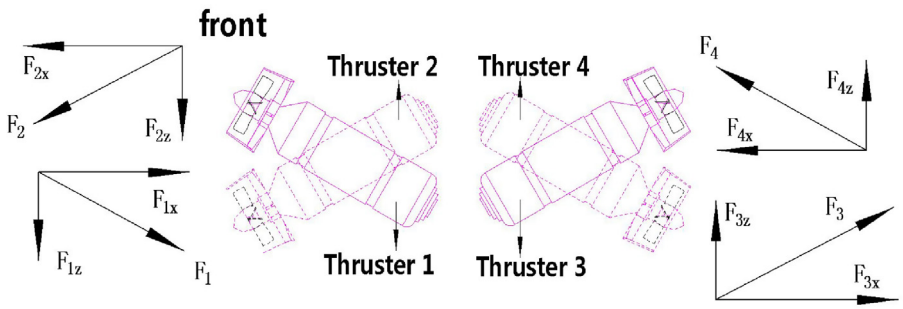

Fig. 8. The pitch and yaw motion.

Table 2
Hydrodynamics coefficients and parameters value.

Thruster angle	$\beta = 15^{\circ}$
The position of the four thrusters	$x_0 = 0.3$, $y_0 = 0.3$, $z_0 = 0$
The center of gravity	CoG : (0, 0, 0)
The center of buoyancy	CoB : (0, 0, − 0.05)
Hydrodynamics coefficients	$X_{\dot{u}} = -0.77$, $X_u = 0$
	$X_{u\|u\|} = -2.45$, $N_{\dot{r}} = -1.99$
	$N_q = 2.59$, $N_r = -6.26$
	$Z_{\dot{w}} = -19.87$, $Z_w = -44.64$
	$Z_p = 13.83$,

simulation by CFD. Parameters in Table 2 is design requirements for the QUUV, such as β, x_0, y_0, CoG and CoB.

6.1. Heave motion

For heave motion higher-order hydrodynamic force is relatively small and can be ignored. Considering $\tau_X = \tau_Y = \tau_K = \tau_M = \tau_N = 0$ and ignoring higher-order hydrodynamic force, the system can be simplified as:

$$\begin{aligned} m\dot{w} &= Z_{\dot{w}}\dot{w} + Z_w w + \tau_Z, \\ \dot{z} &= w, \end{aligned} \tag{25}$$

where $Z_{\dot{w}}$ and Z_w are hydrodynamic coefficients.

Let the sliding-face be:

$$\begin{aligned} \sigma_1 &= \mathbf{h_1^T}[\tilde{w},\ \tilde{z}]^T, \\ \dot{\sigma_1} &= -\eta \tanh(\sigma_1/\rho), \end{aligned} \tag{26}$$

where $\mathbf{h_1}$ is two-dimensional constant vector. Let the desired depth be $3m$ and the others be 0. According to (18) we can obtain:

$$\tau_Z = -59.88 \times 10 \tanh(\sigma_1/0.1) - 111w \tag{27}$$

where $\eta = 10$, $\rho = 0.1$ and $\mathbf{h_1} = [1, 2.6]^T$. The controller can guarantee the heave motion of the underwater vehicle. In addition, it is concluded that $|\tau_Z| = 4|F_{1z}|$ from heave motion analysis because of the same thrusters force. Then it is obtained that $F_1 = F_3 = -F_2 = -F_4 = \frac{\tau_Z}{4\sin(\beta)}$ according to heave motion analysis. If $F_i > 0 (i = 1, 2, 3, 4)$ the thrusters i actuate in the clockwise direction and vice versa.

Figs. 9–11 show heave motion results. Black dashed lines represent the desired values to better understand in these figures. As shown in Fig. 9 the depth reaches the desired value at around 3 s, namely 3 m. The heave speed rises at first to achieve heave motion, which agrees with physical principle. The heave speed declines to the desired value at last, namely 0 m/s. The X and Y position and attitude angle keep zero all the time as depicted in Figs. 10 and 11. It noticed that the theoretically maximum velocity along heave direction can be calculated by $-Z_w w = \tau_{Zmax}$. τ_{Zmax} is the maximum thrusters force along heave direction and is around 41.41 N. The theoretically maximum velocity along heave direction is 0.93 m/s. It can be seen that the maximum heave speed is around 0.9 m/s by Fig. 9, which agrees with theoretical requirements. It is obvious that the QUUV achieves moving in the vertical direction without horizontal direction.

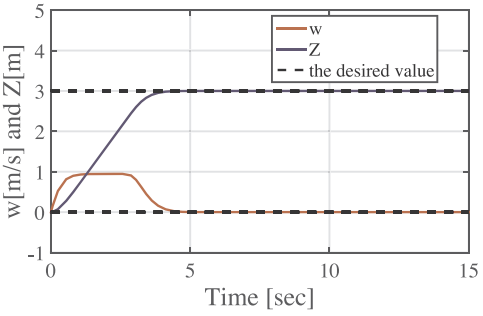

Fig. 9. The speed and depth results for heave motion.

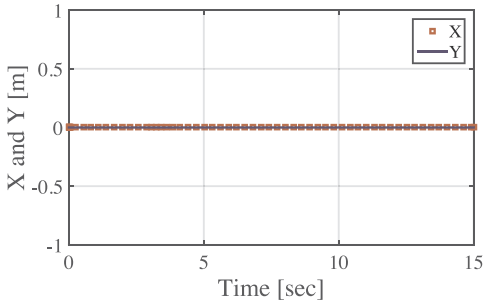

Fig. 10. The X and Y position results for heave motion.

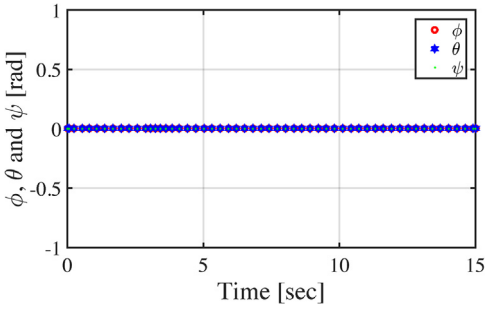

Fig. 11. The attitude angle results for heave motion.

6.2. Surge motion

For surge motion because $\tau_Y = \tau_Z = \tau_K = \tau_M = \tau_N = 0$, the system can be simplified as:

$$m\dot{u} = X_{\dot{u}}\dot{u} + X_u u + X_{|u|u}|u|u + \tau_X \tag{28}$$

where m is the mass of the vehicle, $X_{\dot{u}}$ is hydrodynamic added mass, X_u is linear damping and $X_{|u|u}$ is quadratic damping.

Let the sliding-face be:

$$\sigma_2 = u - u_d \tag{29}$$

where u_d is the desired surge speed. Here u_d is $2m/s$. According to (18) we can obtain the control force:

$$\tau_X = -40.77 \times 2 \tanh(\sigma_2/0.1) + 2.45u|u| \tag{30}$$

where $\eta = 2$ and $\rho = 0.1$. The controller can guarantee the surge motion of the underwater vehicle. In addition, it is concluded that $|\tau_X| = 4|F_{1x}|$ from surge motion analysis because of the same thrusters force. Then it is obtained that $F_3 = F_4 = -F_1 = -F_2 = \frac{\tau_X}{4\cos(\beta)}$ according to surge motion analysis. If $F_i > 0 (i = 1, 2, 3, 4)$ the thrusters i actuate in the clockwise direction and vice versa.

Figs. 12–14 show surge motion results. Black dashed lines represent the desired values to better understand in these figures. The surge speed converges to the desired values at around 1.5 s, namely 2 m/s. The X

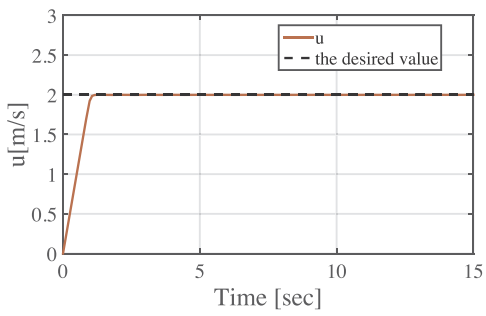

Fig. 12. The surge speed for surge motion.

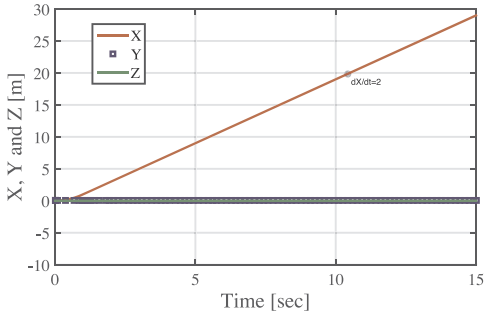

Fig. 13. The position results for surge motion.

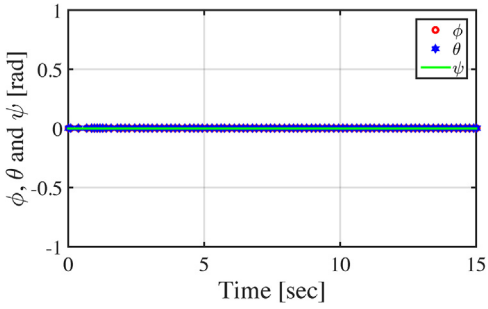

Fig. 14. The attitude angle results for surge motion.

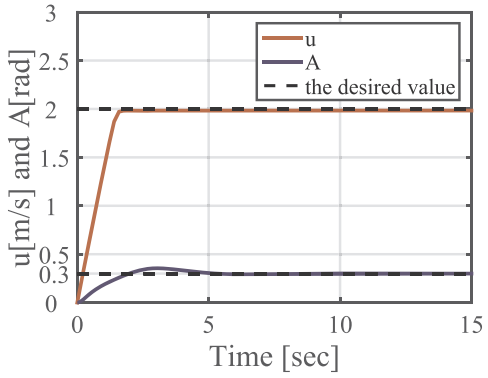

Fig. 15. The surge speed and yaw angle results for space motion.

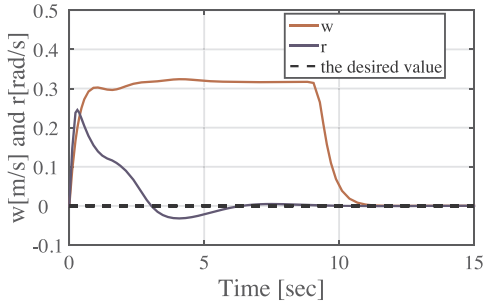

Fig. 16. The heave and yaw speed results for space motion.

position keeps growing because of the surge speed and the gradient of X position is equal to the desired surge speed, namely $2m/s$, as shown in Fig. 13. The Y and Z position and attitude angle hold zero all the time as depicted in Figs. 13 and 14. Apparently, the horizontal motion has nothing to do with vertical motion. The remaining two kinds of motion can be simulated by similar way and are not repeated.

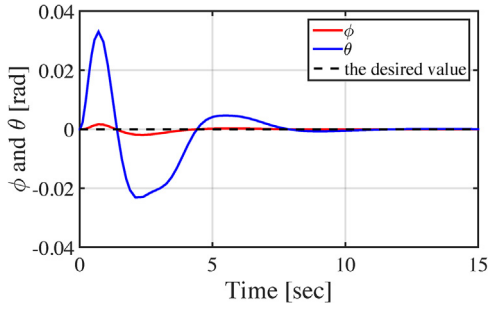

Fig. 17. The attitude angle results for space motion.

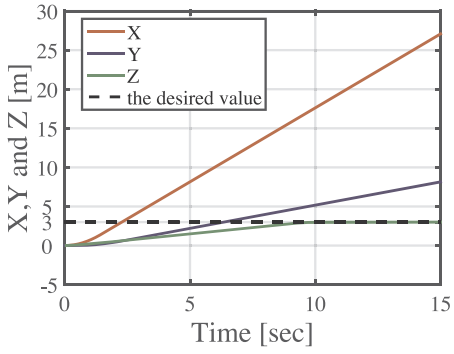

Fig. 18. The position results for space motion.

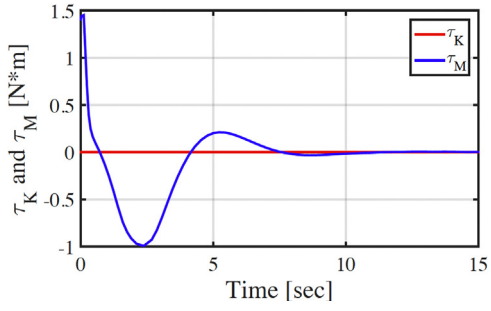

Fig. 19. The τ_K and τ_M results for space motion.

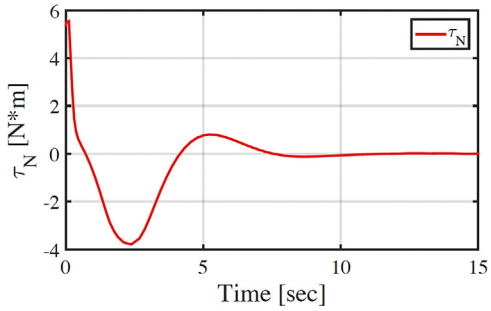

Fig. 20. The τ_N results for space motion.

6.3. Space motion

In general, the three-dimensional space motion is always cruise motion for all kinds of underwater vehicles including multi-thruster AUV, namely moving at the desired speed, yaw angle and depth. It is noted that $\tau_Y = 0$ according to (5) and (7). In addition, it is noticed that the buoyancy moment can make the pitch angle return to zero as described in pitch and yaw motion analysis before. In fact, the buoyancy moment can counteract part of τ_K and τ_M [30]. If τ_K and τ_M has a little value, the roll and pitch angle will keep a small range variation. In

Fig. 21. The size of the pool.

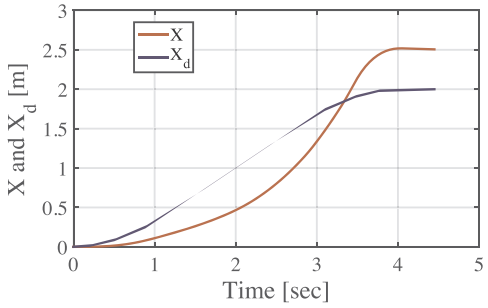

Fig. 22. The actual and desired forward distance results.

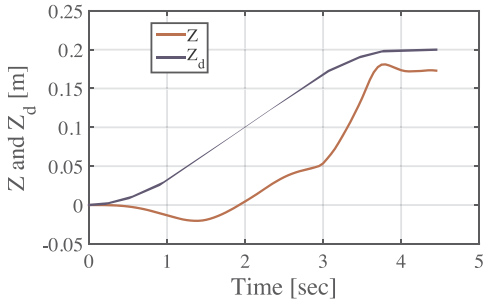

Fig. 23. The actual and desired depth trajectories.

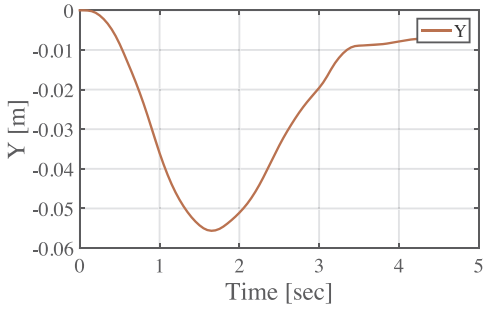

Fig. 24. The sway distance results.

other words, roll and pitch angle can be treated as zero for (3) and (4). Then considering cruise motion requirements and the above contents, the QUUV kinematic equation (1) can be simplified as:

$$\begin{aligned} \dot{z} &= w, \\ \dot{\psi} &= r. \end{aligned} \tag{31}$$

Further ignoring the cross-flow and higher-order hydrodynamic force, the QUUV dynamics equation (5) can be simplified as:

$$\begin{aligned} m\dot{u} &= X_{\dot{u}}\dot{u} + \mathbf{B}_1\mathbf{u}, \\ m\dot{w} &= Z_{\dot{w}}\dot{w} + Z_w w + Z_p p + \mathbf{B}_3\mathbf{u}, \\ I_z\dot{r} &= N_{\dot{r}}\dot{r} + N_r r + \mathbf{B}_6\mathbf{u}, \end{aligned} \tag{32}$$

where $Z_{(\cdot)}$ and $N_{(\cdot)}$ are hydrodynamic coefficients.

With the above notation, the space motion control can be formulated as follows:

Consider the QUUV model with kinematic and dynamic equations given by (31) and (32), respectively. Given the desired u_d, r_d, ψ_d, w_d and z_d, design feedback control laws for the thrusters force $\mathbf{u}$*, such that $u - u_d$, $r - r_d$, $\psi - \psi_d$, $w - w_d$ and $z - z_d$ tend to zero asymptotically.*

Let the sliding-face be:

$$\begin{aligned} \sigma_3 &= u - u_d, \\ \sigma_4 &= (r - r_d) + (\psi - \psi_d), \\ \sigma_5 &= (w - w_d) + 2.6^*(z - z_d), \end{aligned} \tag{33}$$

where $u_d = 2m/s$, $\psi_d = 0.3$, $z_d = 3m$ and the others are 0. It can be seen that from (33):

$$\mathbf{H} = [00100; 01001; 2.60010]^T. \tag{34}$$

It is apparently that $\mathbf{H}_2$ not a square matrix and thereby $\mathbf{u}$ has multiple solutions for Eq. (18). As described in (23) and (24), the method of Lagrange multiplier optimality is adopted for minimizing f with the equality constraint ($\mathbf{H}_2\mathbf{u} = \mathbf{H}_1$). Let $\boldsymbol{\lambda} \in R^{3\times 1}$ be Lagrange multiplier and $\mathbf{U}$ represents $[\mathbf{u};\boldsymbol{\lambda}]$. By Lagrange multiplier optimality, it can be obtained that:

$$\mathbf{CU} = \mathbf{D} \tag{35}$$

where

$$\mathbf{C} = \begin{bmatrix} 2(\mathbf{B}_4^T\mathbf{B}_4 + \mathbf{B}_5^T\mathbf{B}_5) & \mathbf{H}_2^T \\ \mathbf{H}_2 & \mathbf{0}^{3\times 3} \end{bmatrix}, \mathbf{D} = \begin{bmatrix} \mathbf{0}^{4\times 1} \\ \mathbf{H}_1 \end{bmatrix}. \tag{36}$$

Then $\mathbf{U} = \mathbf{C}^{-1}\mathbf{D}$. The thrusters force $\mathbf{u}$ is the first 4 rows of $\mathbf{U}$. It is adopted that $\eta = 2$ and $\rho = 0.1$. The controller can guarantee cruise motion of the underwater vehicle. If $F_i > 0 (i = 1, 2, 3, 4)$ the thrusters i actuate in clockwise direction and vice versa.

Figs. 15–18 show motion results of the three-dimensional space motion controllers. Black dashed lines represent the desired values to better understand in these figures. Fig. 15 shows the surge speed and yaw angle converge to the desired values at around 8 s, namely 2 m/s and 0.3 rad. Fig. 16 shows the heave and yaw speed also converge to desired values at around 12 s, namely 0 m/s and 0 rad/s. As shown in Fig. 17, the roll and pitch angle keep a small range variation around zero, which agrees with assumptions when designing controllers. Fig. 18 shows the depth converges to the desired value at around 8 s, namely 3 m. It is obvious that the X and Y position are in agreement with the yaw angle by observing Fig. 18. Figs. 19 and 20 show moment results (τ_K, τ_M and τ_N). τ_K and τ_M are smaller than τ_N. Considering the buoyancy moment the roll and pitch angle are almost zero, which are in agreement with controller design assumption and verified by Fig. 17. These results demonstrate that the controllers meet space motion requirements and the QUUV can achieve three-dimensional space motion.

Simulation results show the flexibility of the QUUV that successfully makes various motion. Specially, the horizontal and vertical motion are independent for the QUUV. In addition, it is worth of noting that the QUUV model in the simulation is nonlinear and adopts higher-order

hydrodynamic coefficients, such as second-order and coupled hydrodynamic coefficients in contrasts with the linearized model in the controller design. It is admitted that external environment is treated as calm water in the simulation where flows and waves are not considered. It is still obvious that the sliding mode control is a good tool to ensure stability to uncertain parameters and disturbance for the QUUV.

7. Experiment test

An experiment test carried out in a small pool has been made to validate the basic motion function of the proposed QUUV. The pool is 4 m long, 2 m wide and 0.8 m high as shown in Fig. 21. The underwater environment is treated as calm water, although there is often water wave because of wind and other reasons. Considering the pool is too small to make sway motion, forward and downward motions are tested.

In details, the QUUV moves to the desired forward distance (X_d) and depth (Z_d) with the sliding mode controller in the experiment test. The space position and the corresponding speed are obtained by integrating the 3-axis acceleration provided by AHRS. The desired forward distance and depth are 2 m and 0.2 m. In addition, a simple path planning is implemented to obtain better maneuverability, namely

$$X_d(t) = -0.0625t^3 + 0.375t^2,$$
$$Z_d(t) = -0.00625t^3 + 0.0375t^2 \quad (37)$$

where t represents the time and $0\,s \le t \le 4\,s$. When $t \ge 4\,s$, $X_d = 2$ and $Z_d = 0.2$.

Figs. 22–24 show experiment results. As shown in Fig. 22, the red curve and blue curve represent the actual and desired forward distance over time respectively. The actual forward distance gradually increases until the time reach to around fourth second, which is in agreement with the desired forward distance. There exists a deviation of 0.5 m between the final actual and desired forward distance. As stated in Section 6, hydrodynamics coefficients is obtained with numerical computation simulation by CFD, which makes model parameters for the QUUV inaccuracy. In addition, it is noted that the sampling frequency of the AHRS is 20 Hz, which is limited because of its low cost. Placement position of the AHRS should also coincide with the origin of the vehicle-fixed coordinate. In piratical applications, the AHRS is only near the origin of the vehicle-fixed coordinate. As a physical instrument, the AHRS has to carry some errors, such as axis misalignment, fixed bias, drift bias, and so on. Considering these reasons, the sensor, namely the AHRS, is low precision and causes a relatively large cumulative errors. Considering the reasons mentioned above, the deviation is tolerant and the QUUV achieves moving to the desired forward position.

As shown in Fig. 23, the red curve and blue curve represent the actual and desired downward distance over time respectively. It is noticed that the QUUV has an unreasonable ascending motion between 0 s and 1.5 s. It is because sensor accuracy and water wave lead to large vertical acceleration and position error, which makes the controller generates error results. Because of strong robustness of sliding mode control, the actual downward distance approximate converges to 0.17 m at fourth second. There is a deviation of 0.03 m between the final actual and desired downward distance. The QUUV as well achieves moving to the desired downward position. By observing Figs. 22 and 23, the actual process of moving forward and downward is slightly inconsistent with the desired process of moving forward and downward, which is caused together by model parameters accuracy and sensors accuracy.

Fig. 24 shows the trajectory in sway motion which should be kept zero according to experiment requirements. There also exists the deviation because of model parameters accuracy and sensors accuracy. The maximum deviation is 0.055 m and relatively small in comparison with the desired forward distance (2 m) and depth (0.2 m). In addition, the sway distance converges to around −0.008 m at last, and it is also very small in comparison with the desired forward distance and depth. The sway distance can be treated as zero all the time, which is in agreement with motion requirements. These results demonstrate the QUUV achieve motion goal considering limited hardware conditions. The basic motion function is verified for the QUUV.

8. Conclusion

A quadrotor-like unmanned underwater vehicle (QUUV) is designed and implemented in this paper. The most important feature of the QUUV is the four thrusters configured as X shape. The new kind of vehicle is modeled and analyzed. Its motion analysis is discussed in order to show the benefits of setting the four thrusters as an X shape. Its horizontal and vertical motion are independent with four thrusters as X shape. Various motion is simulated based on sliding mode controllers. The QUUV achieves moving forward and downward at the same time with sliding mode controllers in a pool experiment. It is admitted that the shape along heave is not streamlined and it may produce large resistance for heave motion. The shape of the QUUV can be optimized and further studied. The results show the quadrotor-like unmanned underwater vehicle might be a useful tool to explore vast ocean.

Appendix A. Supplementary data

Supplementary data associated with this article can be found, in the online version, at https://doi.org/10.1016/j.apor.2018.06.017.

References

[1] Y. Zhang, J.P. Ryan, J.G. Bellingham, J.B.J. Harvey, R.S. Mcewen, Autonomous detection and sampling of water types and fronts in a coastal upwelling system by an autonomous underwater vehicle, Limnol. Oceanogr. Methods 10 (11) (2012) 934–951, http://dx.doi.org/10.4319/lom.2012.10.934.
[2] K. Asakawa, J. Kojima, Y. Kato, S. Matsumoto, N. Kato, T. Asai, T. Iso, Design concept and experimental results of the autonomous underwater vehicle AQUA EXPLORER 2 for the inspection of underwater cables, Adv. Robot. 16 (1) (2012) 27–42, http://dx.doi.org/10.1163/156855302317413727.
[3] B. Allotta, S. Baines, F. Bartolini, F. Bellavia, Design of a modular autonomous underwater vehicle for archaeological investigations, Oceans (2015), http://dx.doi.org/10.1109/OCEANSGenova.2015.7271398.
[4] D.R. Yoerger, J. Newman, J.J.E. Slotine, Supervisory control system for the JASON ROV, IEEE J. Ocean. Eng. 11 (3) (1986) 392–400, http://dx.doi.org/10.1109/JOE.1986.1145191.
[5] M. Hattori, Scientific applications of the Deep Rov Dolphin-3K, Oceans (1989) 771–776, http://dx.doi.org/10.1109/OCEANS.1989.586678.
[6] B. Allen, R. Stokey, T. Austin, N. Forrester, REMUS: a small, low cost AUV; system description, field trials and performance results, OCEANS'97 MTS/IEEE Conference Proceedings, Vol. 2, IEEE, 1997, pp. 994–1000, , http://dx.doi.org/10.1109/OCEANS.1997.624126.
[7] B.H. Jun, J.Y. Park, F.Y. Lee, P.M. Lee, C.M. Lee, K. Kim, Y.K. Lim, J.H. Oh, Development of the AUV 'ISiMI' and a free running test in an Ocean Engineering Basin, Ocean Eng. 36 (1) (2009) 2–14, http://dx.doi.org/10.1109/OCEANSE.2007.4302335.
[8] S.K. Choi, J. Yuh, G.Y. Takashige, Development of the omnidirectional intelligent navigator, IEEE Robot. Autom. Mag. 2 (1) (1995) 44–53.
[9] H.T. Choi, A. Hanai, S.K. Choi, J. Yuh, Development of an underwater robot, 2003 IEEE/RSJ International Conference on Intelligent Robots and Systems, 2003 (IROS 2003), Proceedings, ODIN-III, vol. 1, IEEE, 2003, pp. 836–841, , http://dx.doi.org/10.1109/IROS.2003.1250733.
[10] F. Pierrot, M. Benoit, P. Dauchez, Optimal thruster configuration for omni-directional underwater vehicles. SamoS: a Pythagorean solution, OCEANS'98 Conference Proceedings, vol. 2, IEEE, 1998, pp. 655–659, , http://dx.doi.org/10.1109/OCEANS.1998.724320.
[11] J. Yuh, M. West, Underwater robotics, Adv. Robot. 15 (5) (2001) 609–639, http://dx.doi.org/10.1163/156855301317033595.
[12] G. Griffiths, Technology, Applications of Autonomous Underwater Vehicles, CRC Press, 2003, http://dx.doi.org/10.1201/9780203522301.
[13] B. Siciliano, O. Khatib, Springer Handbook of Robotics, Springer Science & Business Media, 2008, http://dx.doi.org/10.1007/978-3-540-30301-5.
[14] J. Eastgate, R. Goddard, Submersible aircraft concept design study, 11th International Conference on Fast Sea Transportation, FAST 2011 (2011) 813–820.
[15] X. Yang, J. Liang, T. Wang, G. Yao, W. Zhao, Q. Shen, Submersible unmanned aerial vehicle concept design study, 2013 Aviation Technology, Integration, and Operations Conference (2013).
[16] X. Yang, J. Liang, T. Wang, G. Yao, Computational simulation of a submersible unmanned aerial vehicle impacting with water, 2013 IEEE International Conference on Robotics and Biomimetics (ROBIO) (2013) 1138–1143, http://dx.doi.org/10.

1109/ROBIO.2013.6739617.
[17] G.M. Pake, A. Anvar, A feasibility study of design and development of submersible tube launched UAV-robot, 13th International Conference on Control Automation Robotics Vision (ICARCV) (2014) 1615–1620, http://dx.doi.org/10.1109/ICARCV.2014.7064557.
[18] P.L.J. Drews, A.A. Neto, M.F.M. Campos, Hybrid unmanned aerial underwater vehicle: modeling and simulation, 2014 IEEE/RSJ International Conference on Intelligent Robots and Systems (IROS 2014) (2014) 4637–4642, http://dx.doi.org/10.1109/IROS.2014.6943220.
[19] T. Ranganathan, A. Thondiyath, S.P.S. Kumar, Design and analysis of an underwater quadrotor - AQUAD, Underwater Technology (UT), 2015, IEEE, 2015, pp. 1–5, , http://dx.doi.org/10.1109/UT.2015.7108290.
[20] J. Bian, J. Xiang, H. Liang, A quadrotor-like unmanned underwater vehicle, Control and Decision Conference (CCDC), 2016 Chinese, IEEE, 2016, pp. 6360–6365, , http://dx.doi.org/10.1109/CCDC.2016.7532143.
[21] T.T.J. Prestero, Verification of a Six-Degree of Freedom Simulation Model for the REMUS Autonomous Underwater Vehicle (Ph.D. thesis), Massachusetts institute of technology, 2001.
[22] J. Feldman, DTNSRDC Revised Standarrd Submarine Equations of Motion, Tech. rep., DTIC Document, (1979).
[23] T.I. Fossen, Guidance and Control of Ocean Vehicles Vol. 199 Wiley, New York, 1994.
[24] J. Yuh, Design and control of autonomous underwater robots: a survey, Auton. Robots 8 (1) (2000) 7–24.
[25] A.J. Healey, D. Lienard, Multivariable sliding mode control for autonomous diving and steering of unmanned underwater vehicles, IEEE J. Ocean. Eng. 18 (3) (1993) 327–339, http://dx.doi.org/10.1109/JOE.1993.236372.
[26] V. Sankaranarayanan, A.D. Mahindrakar, Control of a class of underactuated mechanical systems using sliding modes, IEEE Trans. Robot. 25 (2) (2009) 459–467, http://dx.doi.org/10.1109/TRO.2008.2012338.
[27] E. Zakeri, S. Farahat, S.A. Moezi, A. Zare, Robust sliding mode control of a mini unmanned underwater vehicle equipped with a new arrangement of water jet propulsions: simulation and experimental study, Appl. Ocean Res. 59 (2016) 521–542, http://dx.doi.org/10.1016/j.apor.2016.07.006.
[28] G. Antonelli, Underwater Robots: Motion and Force Control of Vehicle-Manipulator Systems, Springer Berlin Heidelberg, 2006, http://dx.doi.org/10.1007/11540199.
[29] D. Lienard, Sliding Mode Control for Multivariable AUV Autopilots (ME Degree Thesis), Naval Postgraduate School, 2002.
[30] R. Bhattacharyya, Dynamics of Marine Vehicles, John Wiley & Sons Inc, 1978.